A Robust Electrochemical Sensor Based on Butterfly-shaped Silver Nanostructure for Concurrent Quantification of Heavy Metals in Water Samples

Naseri, Maryam; Mohammadniaei, Mohsen; Ghosh, Koustuv; Sarkar, Subrata; Sankar, Ravi; Mukherjee, Subhankar; Pal, Souvik; Ansari Dezfouli, Ehsan; Halder, Arnab; Qiao, Jixin

Total number of authors:
12

Published in:
Electroanalysis

Link to article, DOI:
10.1002/elan.202200114

Publication date:
2023

Document Version
Publisher's PDF, also known as Version of record

Research Article Wiley Online Library ELECTROANALYSIS

doi.org/10.1002/elan.202200114

A Robust Electrochemical Sensor Based on Butterfly-shaped Silver Nanostructure for Concurrent Quantification of Heavy Metals in Water Samples

Maryam Naseri,*[a] Mohsen Mohammadniaei,[a] Koustuv Ghosh,[b] Subrata Sarkar,[b] Ravi Sankar,[b] Subhankar Mukherjee,[b] Souvik Pal,[b] Ehsan Ansari Dezfouli,[a] Arnab Halder,[a] Jixin Qiao,[c] Nabarun Bhattacharyya,[b] and Yi Sun*[a]

Abstract: Heavy metals in drinking water have become a severe threat to human health. Detection of heavy metals has been achieved by electrochemical sensors that are modified with complex nanocomposites; however, reproducibility of these sensors is still a big challenge when applied in commercial settings. Here, a simple, very robust, and sensitive electrochemical sensor based on a screen-printed carbon electrode modified with butterfly-shaped silver nanostructure (AgNS/SPCE) has been developed for the concurrent determination of cadmium (II), lead (II), copper (II), and mercury (II) in water samples. The electrochemical behavior of the modified electrodes was investigated using cyclic voltammetry and differential pulse anodic stripping voltammetry. The AgNS/SPCE showed distinct peak potentials and a significant increase in the peak currents for all heavy metals, attributed to the high electrical conductivity and electrocatalytic activity of the synthesized butterfly-shaped AgNS. Moreover, the excellent stability and sensitivity towards simultaneous quantification of heavy metals have been obtained with detection limits of 0.4 ppb, 2.5 ppb, 7.3 ppb, and 0.7 ppb for Cd (II), Pb (II), Cu (II), and Hg (II), respectively. Besides, the constructed sensor was successfully applied to simultaneously quantify target heavy metals in spiked water samples. Owing to excellent sensitivity, high robustness, affordability, and fast response, the presented electrochemical sensor could be incorporated into a portable and miniaturized potentiostat device, making it a promising method for on-site water analysis.

Keywords: Heavy metals · screen-printed carbon electrode · silver nanostructure · differential pulse anodic stripping voltammetry · concurrent detection

1 Introduction

In recent years, due to the increase of industrialization, heavy metals in drinking water have become a sever threat to the environment and human health [1]. Some heavy metals, such as lead, cadmium, and mercury have severe deleterious effect on human health even at very low concentrations. Their exposure can cause kidney problems, attention deficit disorder, learning disorders, and carcinogenicity [2–4]. There are some heavy metals like copper that are necessary nutrient for healthiness in trace levels, whereas high amount can lead to serious health hazards in living organisms. For instance, copper poisoning may cause gastrointestinal hemorrhage, intravascular haemolysis, methaemoglobinaemia, and oliguria [5]. Therefore, international organizations decided to set permissible levels of these heavy metals in drinking water [6]. For example, world health organization (WHO) guidelines set cadmium contents at 0.003 ppm, lead at 0.01 ppm, copper at 2.00 ppm and mercury at 0.006 ppm as permissible levels in drinking water [6].

Considering serious hazardous effects of heavy metals, a sensitive and on-site quantification technique is required for their continuous monitoring. Several traditional techniques such as atomic absorption spectrometry [7], inductively coupled plasma mass spectrometry [8], high performance liquid chromatography inductively coupled plasma mass spectrometry [9] and surface enhanced Raman spectroscopy [10] have been developed as the

[a] M. Naseri, M. Mohammadniaei, E. Ansari Dezfouli, A. Halder, Y. Sun
Department of Health Technology, Technical University of Denmark, Kemitorvet, 2800 Kgs, Lyngby, Denmark
E-mail: suyi@dtu.dk
maryn@dtu.dk
[b] K. Ghosh, S. Sarkar, R. Sankar, S. Mukherjee, S. Pal, N. Bhattacharyya
Centre for Development of Advanced Computing (C-DAC) Kolkata, Agri and Environmental Electronics (AEE) Group, Plot E2/1, Block-GP, Sector – V, Salt Lake, Kolkata, West Bengal, 700091, India
[c] J. Qiao
Department of Environmental Engineering, Technical University of Denmark, Bygningstorvet, 2800 Kgs, Lyngby, Denmark

preferred methods for detection of heavy metals. Although accurate results can be obtained, these techniques suffer from some drawbacks like requiring high cost instrumentation, specialized technician and long analysis time as well as involving complicated operation procedures, rendering them unsuitable for on-site and real-time monitoring. Compared with traditional methods, electrochemical methods have been identified as the most promising approach for heavy metals detection because of their simplicity, fast response, portability and low cost for practical applications [11]. Among electrochemical techniques, differential pulse anodic stripping voltammetry (DPASV), has attracted more attention for heavy metal detection because of the advantages of high sensitivity, low detection limit, and the ability of simultaneous detection of metal ions. The composition of electrodes has key effect on the performance of stripping techniques. For many years, mercury-based electrodes were used for the stripping analysis due to their excellent performance like good reproducibility and possibility of amalgam formation [12]. However, because of the intrinsic disadvantage of mercury-based electrodes such as toxicity and instability, various attempts have been made to introduce mercury-free electrodes with good analytical performances and eco-friendly features.

Recently, screen-printed technology has achieved great advancement, allowing for mass fabrication of reproducible and low cost screen-printed electrodes (SPEs) [13]. With the miniaturized size and the capability to be connected to portable devices, SPEs are regarded as suitable electrodes for on-site analysis [14]. Thanks to its noteworthy stability, gold is widely used in the fabrication of SPEs. Some examples of screen-printed gold electrodes (SPGEs) have been already reported for heavy metals detection [15–18]. Wan et al [17]. introduced a sensitive electrochemical sensor based on SPGE/AuNPs for concurrent quantification of lead and copper. Based on square wave anodic stripping voltammetry (SWASV), the AuNPs/SPGE provided good performance for determination of lead and copper in terms of sensitivity and reproducibility. Bernalte et al [15]. reported an innovative methodology based on SPGE for simultaneous determination of three heavy metals including copper, mercury and lead. They employed their methodology for in-field monitoring of the selected heavy metals in the Amazon River. Despite the great practical utility of these electrodes, they are unsuitable for simultaneous determination of cadmium and lead because of overlapping of their peaks [19]. Considering this problem, screen-printed carbon electrodes (SPCEs) have been selected in this work to enable simultaneous detection of these two heavy metals. However, unmodified SPCEs suffer from low sensitivity, poor stability, and lack of reliability [20]. The use of SPCEs modified with nanomaterials have been emerged as promising probes because of their unique features, like larger effective surface area, abundant active sites, and good chemical stability [21,22]. Many related studies indicate that the application of nanomaterials can enhance electrochemical performance of SPCEs in terms of sensitivity and selectivity for heavy metals detection [20,23,24]. On the other hand, silver nanoparticles (AgNPs) have functioned as appropriate materials for electrode surface modification due to their unique properties like excellent conductivity, reflectivity, high surface-to-volume ratio and their ability to absorb and chemisorb, making them promising platforms as catalysts [25,26].

Considering the excellent sensitivity and stability of silver electrode towards simultaneous detection of cadmium and lead [27], here, we constructed an electrochemical sensor based on SPCEs modified with butterfly-shaped silver nanostructure (AgNS) to concurrently quantify cadmium, lead, copper, and mercury in water samples with a high degree of robustness and reproducibility. Since the particle size and the distributed density of AgNS play important roles in silver electrocatalytic activity, we first optimized the electrodeposition condition of AgNS on SPCE. The synthesized butterfly-shaped AgNS provided: (i) two distinct anodic signals with the peak-to-peak separation of 0.253 V for cadmium and lead; and (ii) signal enhancement due to the extended surface area. The significant increase in anodic peak currents of Cd (II) and Pb (II) was attributed to the fact that AgNS facilitated the nucleation process during anodic stripping step. The AgNS/SPCE also showed an excellent stability and sensitivity towards concurrent quantification of four target heavy metal ions with detection limits of 0.4 ppb, 2.5 ppb, 7.3 ppb and 0.7 ppb for Cd (II), Pb (II), Cu (II), and Hg(II), respectively. We could also successfully detect heavy metals in various water samples such as tap water, rainwater, and lake water collected from Denmark and river water collected from India.

2 Experimental

2.1 Chemicals and Reagents

Potassium nitrate (ACS reagent, ≥99.0 %), silver nitrate (ReagentPlus®, ≥99.0 %), sulphuric acid (ACS reagent, 95.0–98.0 %), potassium hexacyanoferrate(II) trihydrate (ACS reagent, 98.5–102.0 %), sodium acetate (≥99 %), and acetic acid (≥99 %) were obtained from Sigma-Aldrich. Cadmium standard solution (1000 mg/l in 0.5 M HNO_3), lead standard solution (1000 mg/l in 0.5 M HNO_3), copper standard solution (1000 mg/l in 0.5 M HNO_3) and mercury standard solution (1000 mg/l in 0.5 M HNO_3) were purchased from Merck. Working standard solutions were daily made by diluting the stock solutions with 0.1 M acetate buffer solution (pH 4.4).

2.2 Apparatus

Electrochemical studies were carried out using Potentiostat/Galvanostat Metrohm Autolab controlled by the NOVA 2.1 software. Screen-printed carbon electrodes with carbon, silver, and carbon as the working (with 4 mm diameter), reference, and counter electrodes materials,

respectively were purchased from Metrohm (C110). The morphology of SPCEs were perused using field emission scanning electron microscopy (FE-SEM) manufactured by Carl Zeiss operating at 10.00 kV.

2.3 Electrodeposition of Silver Nanostructure on Screen-printed Carbon Electrodes (AgNS/SPCE)

First SPCEs were cleaned by immersing in 0.5 M H_2SO_4 solution and applying cyclic voltammetry (CV) via sweeping potential between 0 and 1.2 V until reaching stable cyclic voltammograms. Then silver nanostructure were electrodeposited of on SPCEs using 3.0 mM $AgNO_3$ solution in 0.1 M KNO_3 solution. For electrodeposition of AgNS, we have used two different methods including single and double-potentiostatic programs. In single potentiostatic program, one deposition potential (−0.2 or −0.1 V) was applied for different times (10 or 30 s). In double-potentiostatic program, we applied a nucleation potential (−0.6 V, −0.8 V, −1.0 V, −1.2 V and −1.4 V) for 50 s and then a growth potential of −0.2 V for 200 s. Finally, the AgNS/SPCE was thoroughly washed with distilled water and then dried with N_2 gas. The modified electrodes were kept under vacuum condition to avoid oxidization of AgNS.

2.4 Electrochemical Measurements

The electrochemical behaviour of SPCE and AgNS/SPCE was investigated by cyclic voltammetry using 2.0 mM $K_4[Fe(CN)_6]$ solution in 0.1 M KCl solution with sweeping potential between −0.2 and +0.5 V at a scan rate of 50 mV s^{-1}. The level of heavy metals in buffer or water samples were measured by dropping 100 µl of sample solution on the AgNS/SPCE through DPASV analysis. The effect of deposition potential and deposition time were evaluated to optimize the performance of the sensor. For this goal, electrochemical response of 200 ppb Cd (II) and 200 ppb Pb (II) in 0.1 M acetate buffer solution (pH 4.4) on AgNS/SPCE was evaluated in different deposition potentials (−0.6, −0.7, −0.8, −0.9 and −1.0 V) and deposition times (30, 60, 90, 180, 240, 360 and 450 s). The optimized parameters of DPASV for concurrent detection of Cd (II), Pb (II), Cu (II), and Hg (II) were potential interval −1.1 to +0.9 V; deposition potential, −0.7 V; deposition time, 360 s; step potential, 5 mV; modulation amplitude, 25 mV; modulation time, 50 ms; interval time, 0.5 s; scan rate, 0.01 V/s. Nova 2.1 software was employed to determine the anodic peak potentials and anodic peak currents.

The sensitivity of AgNS/SPCE was investigated using different concentrations of heavy metals ranging from 5 ppb to 300 ppb for Cd (II), Pb (II) and Hg (II) and 50 ppb to 500 ppb for Cu (II). The calibration curves were obtained by plotting the anodic peak currents as the function of heavy metals concentration. The limit of detections (LOD) were achieved based on the slope of the calibration curves and the standard deviation for the blank measurement (3S/N). Besides the sensitivity, repeatability and reusability of AgNS/SPCE were also examined towards heavy metals detection. In order to test the reusability of AgNS/SPCE, the responses of the sensors were recorded for seven successive determination of 200 ppb Cd (II) and 200 ppb Pb (II) in 0.1 M acetate buffer solution (pH 4.4). Prior to the next determination, the AgNS/SPCE surface was cleaned by applying E = 0.5 V for 80 s in acetate buffer pH 4.4 to remove the previous deposits completely. Repeatability of AgNS/SPCE was evaluated by recording the responses of seven individual modified electrodes towards detection of Cd (II) and Pb (II) using 0.1 M acetate buffer solution (pH 4.4) containing 200 ppb Cd (II) and 200 ppb Pb (II).

2.5 Sample Preparation

Water samples were collected from tap water in our lab, rainwater, lake water from Denmark and river water from India. These samples were filtered through a 0.45 mm filter. Generally, 200 µl of 1 M acetate buffer pH 4.4 was mixed with 1.8 ml water sample and then analyzed by the optimized DPASV method. The practical application of AgNS/SPCEs was evaluated by spiking the known amount of Cd (II),

Pb(II), Cu(II), and Hg(II) into the water samples. Then recoveries were calculated using following equation:

$$\text{Recovery } \% = \frac{C_{Found\ by\ calibration\ plots}}{C_{Added}} \times 100$$

3 Results and Discussion

3.1 Electrodeposition of Silver Nanostructure on SPCE

Figure 1 indicates the cyclic voltammogram of SPCE in 0.1 M KNO_3 solution containing 3.0 mM $AgNO_3$. The cyclic voltammogram of $AgNO_3$ showed a cathodic peak and an anodic sharp peak at −0.127 V and +0.126, respectively. Cathodic peak is outcome of the reduction of Ag^+ ions on the surface of electrode, while anodic

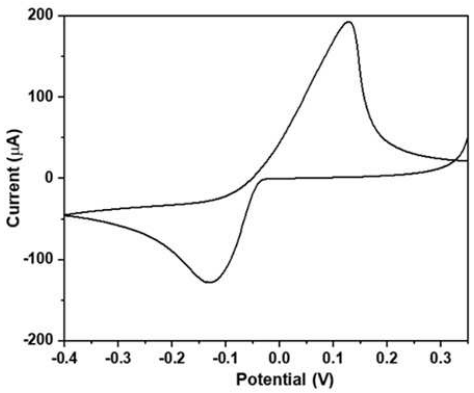

Fig. 1. CV response of SPCE in 0.1 M KNO_3 solution containing 3.0 mM $AgNO_3$ at 50 mVs^{-1}.

peak is attributed to the stripping of the electrodeposited silver [28]. In order to optimize conditions for Ag^+ electrodeposition, two different methods including single and double-potentiostatic programs have been examined. The modified electrodes were evaluated to detect Cd (II) and Pb (II) ions using acetate buffer solution pH 4.4 containing 200 ppb of Cd (II) and 200 ppb Pb (II). In double-potentiostatic program (Figure 2A), the electrode with the nucleation potential of −1.2 V attained the highest anodic peak current for Pb (II) (~3.8 μA), while the highest anodic peak current for Cd (II) (~7.4 μA) appeared at the nucleation potential of −1.4 V. As can be seen in figure 2B for single potentiostatic program, the electrode with the electrodeposition potential of −0.2 V for 30s attained the highest anodic peak current for both Pb (II) (~1.5 μA) and Cd (II) (~9.4 μA).

Moreover, the effect of Ag^+ ion concentration was evaluated by using different concentrations of $AgNO_3$ (0.1, 0.5, 3.0, and 10.0 mM) and applying −0.2 V for 30s. Figure 2C indicates that the current response of Pb (II) increased gradually from ~0.9 μA to ~1.8 μA as concentration of $AgNO_3$ increased from 0.1 to 0.5 mM. However, increasing the Ag^+ concentration higher than 0.5 mM led to slight decrease in the current signal. The current response of Cd (II) enhanced gradually from ~2.1 μA to ~9.0 μA as Ag^+ concentration raised from 0.1 to 0.5 mM, while it was kept nearly constant when increasing Ag^+ concentration to 10.0 mM (Figure 2C). The enhanced current responses of both Pb (II) and Cd (II) could be attributed to enhanced electrical conductivity and high rate electron transfer of the electrode as the amount of AgNP was increased [29,30]. Therefore, the optimal condition for electrodeposition of AgNS on SPCEs was selected using 3.0 mM $AgNO_3$ in 0.1 M KNO_3 solution through the single potentiostatic program with the electrodeposition potential of −0.2 V for 30s.

The surface morphology of SPCEs before and after modification were investigated by FE-SEM. The SEM image of the bare SPCE showed a homogeneous distribution of graphite flakes with a lot of pores which was attributed to the cross-linking agent in the original ink [31](Figure 3A and 3B). The porous structure of SPCE exposes a large surface area, which can provide more adsorption sites and enhance the performance of the electrode for various application. As shown in Figure 3C, a homogenous dispersion of AgNS at SPCE surface was observed after electrodeposition of AgNS on the surface of SPCE under the optimized condition. A high magnification focused on the surface of AgNS/SPCE indicated that the electrodeposited silver nanostructures were mostly butterfly-shaped (Figure 3D) [32]. Moreover, energy dispersive X-ray (EDX) analysis was employed to confirm the presence of AgNS on the surface of SPCE. As shown in Figure 3E, the EDX spectrum proves the presence of Ag, indicating the formation of AgNS on the surface of SPCE.

3.2 Electrochemical Performance of AgNS/SPCE

Electrochemical behaviour of bare and modified SPCE was first studied via CV using 2.0 mM $K_4[Fe(CN)_6]$ solution in 0.1 M KCl solution. It was found that a couple of typical redox peaks of $K_4[Fe(CN)_6]$ appeared at bare SPCE (Figure 4). The redox peaks enhanced at AgNS/

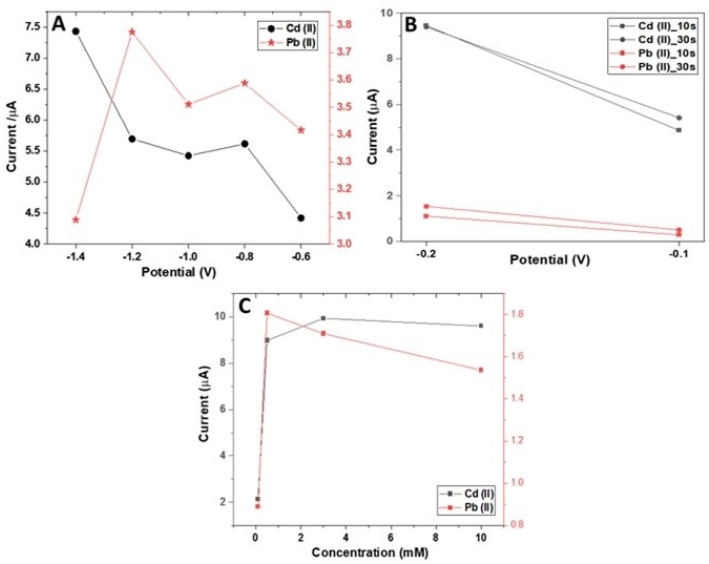

Fig. 2. Peak currents of Cd (II) and Pb (II) using SPCEs modified (A) through the double-potentiostatic program with nucleation potentials of −0.6 V, −0.8 V, −1.0 V, −1.2 V and −1.4 V; (B) through the single potentiostatic program with deposition potentials of −0.2 V and v0.1 V for 10 and 30 s; and (C) through the single potentiostatic program with different concentrations of $AgNO_3$ (0.1, 0.5, 3.0, and 10.0 mM). (All experiments have been done using 0.1 M acetate buffer solution pH 4.4 containing 200 ppm Cd (II) and 200 ppm Pb(II)).

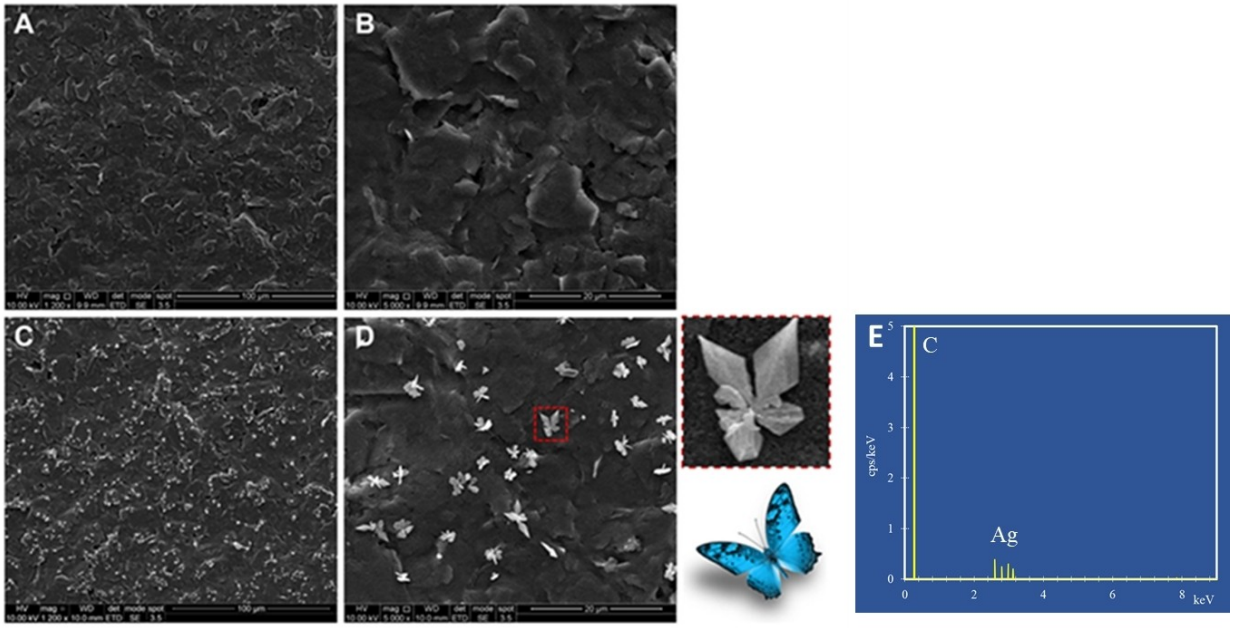

Fig. 3. FE-SEM images of SPCE at 1200X magnification (A) and at 20000X magnification (B) and butterfly-like AgNS/SPCE at 1200X magnification (C) and at 20000X magnification (D). EDX spectrum of AgNS/SPCE (E).

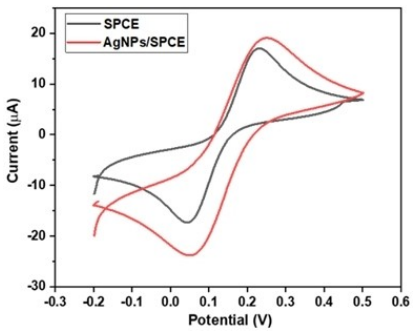

Fig. 4. CV responses of bare and modified SPCE in 0.1 M KCl solution containing 2.0 mM $K_4[Fe(CN)_6]$.

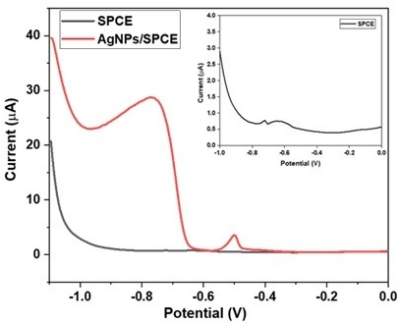

Fig. 5. DPSV responses of Cd (II) and Pb (II) with bare and modified SPCE in 0.1 M acetate buffer solution pH 4.4 containing 200 ppb Cd(II) and 200 ppb Pb(II).

SPCE, suggesting that introducing AgNS provided a better electrochemical catalytic behavior and promoted electron transfer process at the surface of AgNS/SPCE. Figure 5 indicates the anodic stripping voltammograms of the optimized and bare SPCEs using 200 ppb Cd (II) and 200 ppb Pb (II) in 0.1 M acetate buffer solution (pH 4.4). Two weak anodic peaks with the peak-to-peak separation (ΔE_p) of 0.100 V ($E_P = -0.722$ V for Cd (II) and $E_P = -0.622$ V for Pb (II)) were observed on SPCE, while on the AgNS/SPCE, two well-defined anodic peaks appeared with ΔE_p value as 0.253 V ($E_P = -0.747$ V for Cd (II) and $E_P = -0.501$ V for Pb (II)). The anodic peak currents of Cd (II) and Pb (II) were 199 times and 19.2 times higher on AgNP/SPCE compare with bare SPCE. This significant enhancement in the peak currents of Cd (II) and Pb (II) can be attributed to the raising electrical conductivity of the electrodes due to the addition of AgNS. Moreover, AgNS can create fused alloys with heavy metals which making it simplified to be reduced [33,34]. So AgNS would facilitate the nucleation process in anodic stripping step in the same manner for Bi electrodes [33,35].

3.3 DPV Parameter Optimization

In order to obtain the highest signals Cd (II) and Pb (II) for the AgNS/SPCE electrode, the deposition potential and deposition time were optimized. The deposition potential was changed from −0.6 V to −1.0 V with 0.1 V intervals, while the deposition time was set to a constant value of 30s. As seen in figure 6A, the highest peak current was obtained at a deposition potential of −0.7 V for both Pb (II) and Cd (II), which could be attributed to the fact that at this deposition potential, Pb (II) and Cd

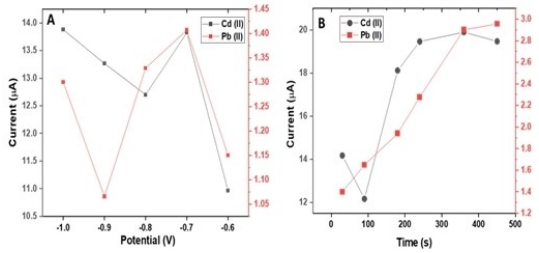

Fig. 6. Peak currents of Cd (II) and Pb (II) using AgNS/SPCEs (A) by applying the deposition potentials of −0.6 V, −0.7 V, −0.8, −0.9 and −1.0 V for 30s; (B) by applying a deposition potential of −0.7 V in different deposition times of 30, 90, 180, 240, 360 and 540s. (All experiments have been done using 0.1 M acetate buffer solution pH 4.4 containing 200 ppb Cd (II) and 200 ppb Pb(II)).

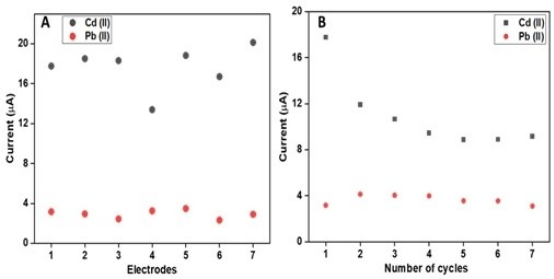

Fig. 7. Peak currents of Cd (II) and Pb (II) (A) using seven different AgNS/SPCE that were prepared independently by the same procedure; (B) using one AgNS/SPCE for seven successive detection of Cd (II) and Pb (II). (All experiments have been done using 0.1 M acetate buffer solution pH 4.4 containing 200 ppb Cd (II) and 200 ppb Pb(II)).

(II) are reduced more efficiently. Thus, the optimal deposition potential of −0.7 V was chosen in this work. Since accumulation of metal ions on the electrode surface can improve the analytical sensitivity of sensor, the deposition time effect on the responses of Pb (II) and Cd (II) ions was studied via applying −0.7 V in different deposition times of 30, 90, 180, 240, 360 and 540s. It can be seen in Figure 6B that the peak currents of mixed ions increased by a factor of 2 when increasing the deposition time from 90 s to 360 s. This can be attributed to increasing the amount of metal ions at the surface of electrodes in longer preconcentration times. With further increase of deposition time, the peak currents of Cd (II) decreased, whereas the Pb (II) peak currents increased gently. It means that the amount of heavy metals at the surface of electrode reached to a threshold because of competitive reaction between ions at the surface of electrode. In order to ensure high sensitivities for both Cd (II) and Pb (II), a deposition time of 360 s was employed as the optimized deposition time in this work.

3.4 Reproducibility and Reusability Study

The reproducibility of AgNS/SPCE was examined with 7 different electrodes that were prepared according to the optimized electrodeposition method (Figure 7A). The relative standard deviation (RSD) values for Pb (II) and Cd (II) were 0.42 % and 2.15 %, respectively, which indicated the reliability of the modified electrodes. Additionally, the reusability of modified electrode was examined by successive detection of 200 ppb Pb (II) and 200 ppb Cd (II) using one AgNS/SPCE (Figure 7B). The results showed the RSD values of 0.42 % for Pb (II) and 3.20 % for Cd (II) for 7 times successive determination, indicating excellent stability of the modified electrode.

3.5 Concurrent Detection of Heavy Metals Using AgNS/SPCE

The detection ability of AgNS/SPCE was tested for concurrent detection of Cd (II), Pb (II), Cu (II) and Hg (II) in 0.1 M acetate buffer (pH 4.4) by DPSV analysis under the optimized conditions.

Figure 8 indicates DPSV responses of the AgNS/SPCE for the simultaneous detection of four target metal ions. As can be seen, four individual peaks in their coexistence appeared at approximately −0.788 V, −0.536 V, −0.209 V, and 0.627 V for Cd (II), Pb (II), Cu (II), and Hg (II), respectively. Besides these four peaks, another anodic peak appeared around 0.028 V which correspond to the oxidation of silver. Distances between the anodic peaks are big enough to facilitate the concurrent determination of four target metal ions using the AgNS/SPCE. The peak shape in Figure 8 is different from that of the single metal ion (Figure 5). The rationale behind the shape differences between the two experiments might be due to having a pseudo-reference electrode, which would affect the signals shapes or locations resulting from different solutions compositions [36]. Although, the observed peak current shapes were different, the values were identical. The anodic peak currents of four ions increased with the increase of their concentrations. The calibration plots were observed to be linear in the range of 5 to 300 ppb for Cd (II), 5 to 300 ppb for Pb (II), 50 to 500 ppb for Cu(II), and 5 to 100 ppb for Hg (II) (Figure 9). The detection limits for Cd (II), Pb (II), Cu (II), and Hg(II) were determined to be 0.4 ppb, 2.5 ppb, 7.3 ppb and 0.7 ppb, respectively. Electrochemical performance of AgNS/SPCE was compared with other reported electrodes for the electrochemical detection of Cd (II), Pb (II), Cu (II), and Hg(II) ions (Table 1). Comparisons showed that the AgNS/SPCE can be a promising platform for the concurrent detection of these heavy metals with high sensitivity and low LOD values. Although the LOD values at the AgNS/SPCE were not the best among the work reported previously, our modified electrode can concurrently provide analysis for four target heavy metals. Moreover, the sensing performance of AgNS/SPCE is good enough for implementation in practice. Additionally, the reproducibility of proposed sensor was estimated with 3 different AgNS/SPCEs that were prepared by the same protocol within a series of 3

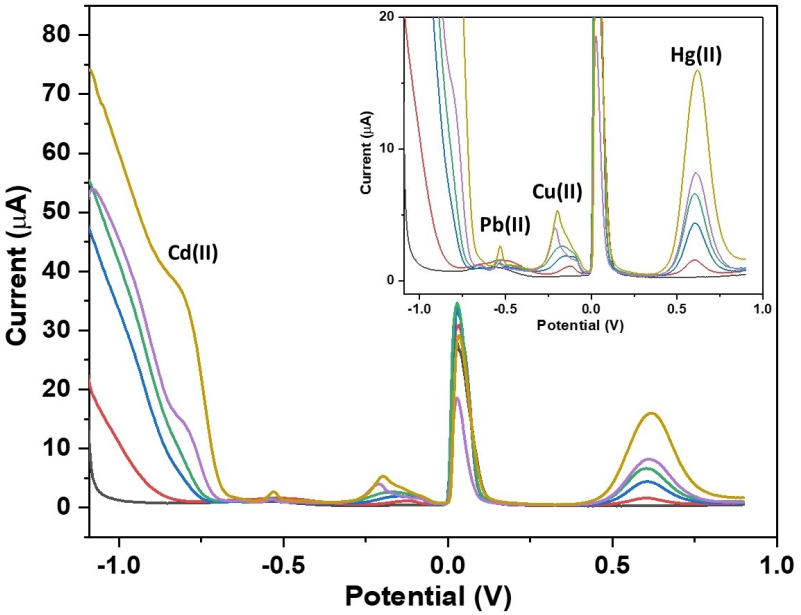

Fig. 8. DPSV responses of AgNS/SPCE using 0.1 M acetate buffer pH 4.4 containing different concentrations of Cd (II), Pb (II), Cu (II) and Hg (II).

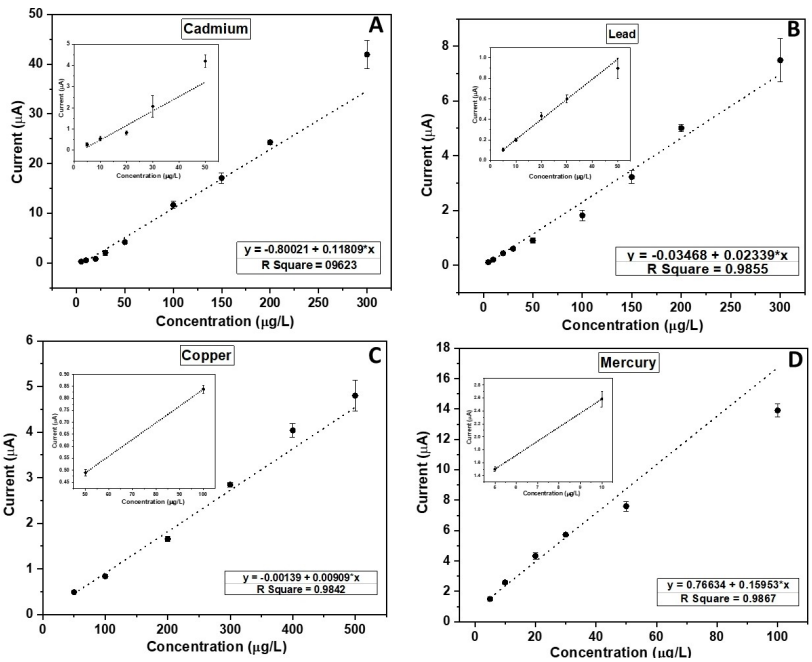

Fig. 9. The calibration plots of (A) Cd (II), (B) Pb (II), (C) Cu (II), and (D) Hg(II) using AgNS/SPCE in presence of different concentrations of four heavy metals.

repetitive measurements (Figure 10) The RSD values for measuring 150 ppb Cd (II), 30 ppb Pb (II), 300 ppb Cu (II) and 30 ppb Hg (II) were 6.9 %, 0.1 %, 3.9 % and 3.9 %, respectively, which demonstrated the reliability of presented sensor for the concurrent detection of these heavy metal ions.

Furthermore, the morphology of the AgNS after detection was investigated to evaluate stability of the AgNS/SPCE during the detection. Figure 11 indicates the SEM image of AgNS/SPCE after concurrent measuring of 150 ppb Cd (II), 30 ppb Pb (II), 300 ppb Cu (II) and 30 ppb Hg (II). A high magnification images of the electrode showed that the electrodeposited silver nanostructures kept their butterfly-shaped after the detection. This demonstrates the stability of the electrodes after a high potential of 0.9 V during the detection.

Table 1. Comparison of the proposed sensor for determination of Cd (II), Pb (II), Cu (II) and Hg (II) with others.

Electrodes	Method	Linear ranges (ppb)	Detection limits (ppb)	Reference
MWCNT/P1,5-DAN	ASV	Cd (II), 4–150	3.20	[37]
		Pb (II), 4–150	2.10	
RGO/Bi/CPE	DPASV	Cd (II), 20–120	2.80	[38]
		Pb (II), 20–120	0.55	
		Cu (II), 20 –100	26.0	
CB-18-crown-6-GEC	DPASV	Cd (II), 7.9–191.1	2.40	[39]
		Pb (II), 5.0–186.5	1.50	
		Cu (II), 5.1–177.3	1.50	
graphene/CeO_2/GCE	DPASV	Cd (II), 22.5–281	0.02	[40]
		Pb (II), 41.4–518	0.02	
		Cu (II), 12.7–158.9	0.01	
		Hg (II), 40.1–501.5	0.05	
NG/GCE	DPSV	Cd (II), 5.6–11.3	5.6	[41]
		Pb (II), 2.1–1864.8	1.0	
		Cu (II), 0.6–317.7	0.3	
		Hg (II), 40.1–1805.3	10.0	
AgNP/GPE	ASV	Cd (II), 184.0- 613.2	17	[30]
		Pb (II), 111.8–745.1	12	
		Cu (II), 94.5–945.4	44	
AgNPs@P-1,8-DAN/GC	ASV	Cd (II), 0.02–337.2	0.019	[33]
		Pb (II), 0.03–2486.4	0.031	
		Cu (II), 0.004–762.5	0.005	
SPCE/CDs/AuNP	DPV	Cd (II), 10–270	2.8	[42]
		Pb (II), 10–270	4.2	
		Cu (II), 10–270	14.0	
Bigareau Burlat kernel shell/CPE	SWV	Cd (II), 9.5–80	9.56	[43]
		100–1000	8.48	
		Pb (II), 8.5–10	9.77	
		100–1000		
		Cu (II), 10–80		
		100–1000		
AgNS/SPCE		Cd (II), 5–300	0.4	This work
		Pb (II), 5–300	2.5	
		Cu (II), 50–500	7.3	
		Hg (II), 5–100	0.7	

MWCNT: multiwalled carbon nanotubes; P1,5-DAN: poly(1,5-diaminonaphthalene); CPE: Carbon paste electrode; GEC: graphite-epoxy composite; NG: N-doped graphene; GPE: Graphene Paste Electrode; P-1,8-DAN: poly(1,8-diaminonaphthalene); CDs: Carbon dots.

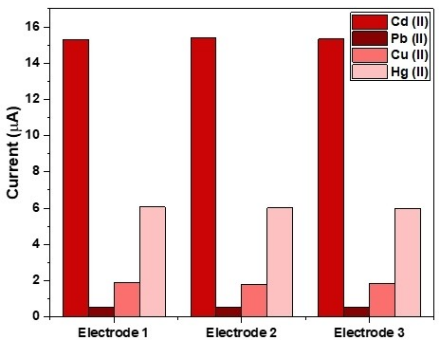

Fig. 10. Peak currents of Cd (II), Pb (II), Cu (II) and Hg (II) using three different AgNS/SPCE that were prepared independently by the same procedure.

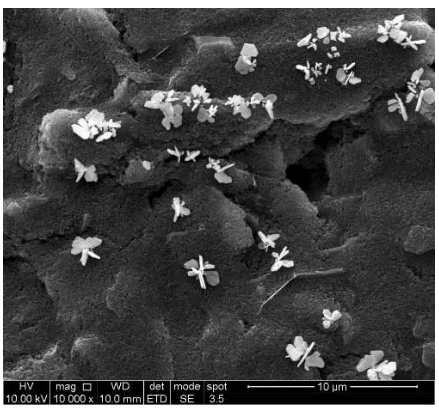

Fig. 11. FE-SEM images of butterfly-like AgNS/SPCE after detection at 10000X magnification.

3.6 Practical Application of AgNS/SPCE

In order to examine the applicability of the developed electrode, some water samples were collected from four different sources including tap water from our lab, rainwater from Denmark, lake water from Denmark and river water from India. ICP-MS analysis of the collected samples revealed the amount of Cd (II), Pb(II), and Hg(II) were less than 0.01 ppb and Cu(II) level was less than 0.1 ppb. Therefore, spiking the known amount of Cd (II), Pb(II), Cu(II), and Hg(II) into the water samples was employed to examine the practical application of AgNS/SPCEs. The pH of samples was adjusted to pH 4.4 with 1 M acetate buffer prior to determination and the optimal conditions were used for heavy metals detection in these experiments. As shown in Table 2 and 3, the average recoveries range from 90.6 % to 110.3 % for Cd (II), 90.38 % to 110.36 % for Pb(II), 90.0 % to 110.5 % for Cu(II), and 90.1 % to 113.1 % for Hg(II). The obtained recoveries values indicated that AgNS/SPCE can be a promising electrode for simultaneous detection of Cd (II), Pb(II), Cu(II), and Hg(II) in water samples.

4 Conclusions

In this work, we developed a reliable and sensitive electrochemical sensor towards simultaneous detection of four heavy metals of cadmium (II), lead (II), copper (II), and mercury (II). Regarding to the problem that can be encountered in the simultaneous analysis of cadmium and lead ions, SPCE modified with butterfly-shaped AgNS was employed as a very promising probe. Key analytical factors such as electrodeposition condition of AgNS and DPV parameters were optimized towards simultaneous detection of Cd (II) and Pb (II). Due to the excellent electrical conductivity and high electrocatalytic activity of AgNS, two distinguished anodic signals with the peak-to-peak separation of 0.253 V were recorded for Cd (II) and Pb (II)) on AgNS/SPCE. With very low detection limits and high signal reproducibility, the presented AgNS/SPCE sensor was also able to successfully measure the four heavy metal ions in four different water samples with excellent recoveries. The further investigation is being considered to incorporate the fabricated sensor into a portable and miniaturized potentiostat device that can

Table 2. Recovery result for Cd(II) and Pb(II) in four different water samples using Ag/SPCE (n = 3).

	Added /ppb	Pb		Cd	
		Found /ppb	Recovery%	Found /ppb	Recovery%
Tab water	10	9.04 ± 0.39	90.38	9.15 ± 0.32	91.5
	30	29.46 ± 0.04	98.21	29.49 ± 0.97	98.3
	100	93.69 ± 1.20	93.69	102.97 ± 1.55	103
Rainwater	10	9.68 ± 0.40	96.79	10.05 ± 0.34	100.5
	30	27.62 ± 0.80	92.05	27.2 ± 0.84	90.7
	100	96.84 ± 1.69	96.84	110.27 ± 1.51	110.3
Lake water	10	10.32 ± 0.42	103.21	10.8 ± 0.41	108
	30	27.72 ± 0.21	92.41	27.21 ± 0.05	90.7
	100	90.78 ± 1.45	90.78	103.54 ± 0.95	103.5
River water	10	9.27 ± 0.08	92.71	9.06 ± 0.17	90.6
	30	33.11 ± 0.75	110.36	29.59 ± 0.51	98.6
	100	109.22 ± 1.36	109.22	109.17 ± 0.84	109.2

Table 3. Recovery result for Cu(II) and Hg(II) in four different water samples using Ag/SPCE (n = 3).

	Hg			**Cu**		
	Added /ppb	Found /ppb	Recovery%	Added /ppb	Found /ppb	Recovery%
Tab water	10	9.06 ± 0.41	90.6	50	52.98 ± 0.52	106
	30	30.77 ± 1.12	102.6	100	109.04 ± 2.31	109
	50	53.31 ± 1.44	106.6	300	331.64 ± 2.64	110.5
Rainwater	10	10.49 ± 0.53	104.9	50	51.79 ± 0.73	103.6
	30	32.56 ± 1.05	108.5	100	90.03 ± 1.76	90.0
	50	45.07 ± 1.35	90.1	300	271.69 ± 1.65	90.6
Lake water	10	9.09 ± 0.019	90.9	50	53.4 ± 0.42	106.8
	30	31.29 ± 0.85	104.3	100	90.59 ± 1.97	90.6
	50	56.56 ± 1.03	113.1	300	273.71 ± 2.62	91.2
River water	10	9.03 ± 0.09	90.3	50	49.07 ± 0.27	98.1
	30	32.71 ± 0.93	109	100	90.31 ± 1.35	90.3
	50	55.16 ± 0.26	110.3	300	271.83 ± 2.64	90.6

facilitate on-site water safety analysis. The developed platform can be greatly employed for electrochemical detection of other biomarkers with high degree of sensitivity and reproducibility.

Acknowledgements

This endeavor has been performed in the Indo-Danish Research and Innovation Cooperation in the Area of Water. Authors acknowledge the joint funding by Innovation Fund Denmark [8127-00021B], and the Department of Biotechnology (DBT), Government of India [Grant ID: BT/IN/DENMARK/62/NB/2018-19 (PFMS), dated 23/03/2019].

Data Availability Statement

The data that support the findings of this study are available from the corresponding author upon reasonable request.

References

[1] S. Bolisetty, M. Peydayesh, R. Mezzenga, *Chem. Soc. Rev.* **2019**, *48*, 463.
[2] A. Kumar, A. Kumar, A. K. Chaturvedi, *Int. J. Environ. Res. Public Health* **2020**, *17*, 2179.
[3] F. Khan, S. Momtaz, M. Abdollahi, *J. Trace Elem. Med. Biol.* **2019**, *52*, 37–47.
[4] G. Fatima, A. Mehdi, R. Najah, H. Nitu, *Indian J. Clin. Biochem.* **2019**, *34*, 371–378.
[5] L. M. Gaetke, C. Kuang, *Toxicology* **2003**, *189*, 147–163.
[6] S. Mukherjee, S. Bhattacharyya, K. Ghosh, N. B. Pal, S. Arnab Halder, M. Naseri, M. Mohammadniaei, S. Sarkar, A. Ghosh, Y. Sun, *Trends Food Sci. Technol.* **2021**, *109*, 674–689.
[7] E. D. C. C. Radulescu, I. D. Dulama, C. Stihi, I. Ionita, A. Chilian, C. Necula, *Rom. J. Phys.* **2014**, *59*, 1057–1066.
[8] S. H. Choi, J. Y. Kim, E. M. Choi, M. Y. Lee, J. Y. Yang, H. Lee, K. S. Kim, J. Yang, R. E. Russo, J. H. Yoo, J. Kang, K. S. Park, S. Hwa, J. Y. Kim, E. M. Choi, M. Y. Lee, J. Y. Yang, G. H. Lee, K. S. Kim, J. Yang, R. E. Russo, J. H. Yoo, *Anal. Lett.* **2019**, *52*, 496–508.
[9] J. Vogl, K. G. Heumann, *Fresenius J. Anal. Chem.* **1997**, *359*, 438–441.
[10] D. K. Sarfo, A. Sivanesan, E. L. Izake, G. A. Ayoko, *RSC Adv.* **2017**, *7*, 21567–21575.
[11] A. Khanmohammadi, A. Jalili, G. Pegah, H. Abbas, A. Fabiana, *J. Iran. Chem. Soc.* **2020**, *17*, 2429–2447.
[12] L. Clóvis, S. Jorge, *Fresenius J. Anal. Chem.* **2000**, *367*, 284–290.
[13] D. Maddipatla, B. B. Narakathu, *Biosensors* **2020**, *10*, 199.
[14] S. Electrodes, T. Application, *Sensors* **2016**, *16*, 1761.
[15] E. Bernalte, S. Arévalo, J. Pérez-taborda, J. Wenk, P. Estrela, A. Avila, M. Di, *Sens. Actuators B* **2020**, *307*, 127620.
[16] S. M. Silva, A. L. Squissato, D. P. Rocha, M. L. S. Vasconcellos, R. D. Q. Ferreira, E. M. Richter, R. A. A. Munoz, *Ionics* **2020**, *26*, 2611–2621.
[17] H. Wan, Q. Sun, H. Li, F. Sun, N. Hu, P. Wang, *Sens. Actuators B* **2015**, *209*, 336–342.
[18] S. Laschi, I. Palchetti, M. Mascini, *Sens. Actuators B* **2006**, *114*, 460–465.
[19] T. Lead, J. Wang, B. Tian, *Electroanalysis* **1993**, *5*, 809–814.
[20] N. Jeromiyas, E. Elaiyappillai, A. Senthil, *J. Inst. Chem.* **2019**, *95*, 466–474.
[21] G. E. Uwaya, O. E. Fayemi, *J. Cluster Sci.* **2021**, *7*, 8–10.
[22] Q. Khue, Q. Huy, N. Phan, T. Anh, T. Thanh, L. Dang, *Mater. Today Commun.* **2021**, *26*, 101726.
[23] H. Wang, Y. Yin, G. Zhao, F. Bienvenido, I. M. Floresparrad, Z. Wang, G. Liu, *Int. J. Agric. Biol.* **2019**, *12*, 194–200.
[24] J. M. D.-C. María A. Tapia, C. Pérez-Ràfols, R. Gusmão, N. Serrano, Z. ˇek Sofer, *Electrochim. Acta* **2020**, *362*, 137144.
[25] M. S. Shivakumar, G. Krishnamurthy, C. R. Ravikumar, A. S. Bhatt, *J. Sci. Adv. Mater. Devices* **2019**, *4*, 290–298.
[26] L. Kvı, R. Vec, *J. Phys. Chem. B* **2006**, *110*, 16248–16253.
[27] K. H. Schrùder, *Electroanalysis* **2001**, *13*, 1–6.
[28] S. Wu, H. Zhao, H. Ju, C. Shi, J. Zhao, *Electrochem. Commun.* **2006**, *8*, 1197–1203.
[29] M. Pumera, A. E. Ã, *Electrophoresis* **2009**, *30*, 3315–3323.
[30] S. Palisoc, E. T. Lee, M. Natividad, L. Racines, *Int. J. Electrochem. Sci.* **2018**, *13*, 8854–8866.
[31] X. Niu, C. Chen, H. Zhao, J. Tang, Y. Li, M. Lan, *Electrochem. Commun.* **2012**, *22*, 170–173.
[32] C. Yang, X. Xiang, Y. Zhang, Z. Peng, Z. Cao, *Sci. Rep.* **2015**, *5*, 12355.
[33] K. M. Hassan, G. M. Elhaddad, M. AbdelAzzem, *Microchim. Acta* **2019**, *186*, 440.
[34] F. E. Salih, A. Ouarzane, M. El Rhazi, *Arab. J. Chem.* **2017**, *10*, 596–603.
[35] J. Wang, *Electroanalysis* **2005**, *17*, 1341.
[36] L. Kashefi-Kheyrabadi, J. Kim, S. Chakravarty, S. Park, H. Gwak, S.-I. Kim, M. Mohammadniaei, M.-H. Lee, K.-A. Hyun, H.-I. Jung, *Biosens. Bioelectron.* **2020**, *169*, 112622.
[37] H. D. Vu, L. Nguyen, T. D. Nguyen, *Ionics* **2015**, *21*, 571–578.
[38] P. K. Sahoo, B. Panigrahy, S. Sahoo, A. K. Satpati, D. Li, D. Bahadur, *Biosens. Bioelectron.* **2013**, *43*, 293–296.
[39] N. Serrano, A. González-calabuig, *Talanta* **2015**, *138*, 130–137.
[40] Y. Xie, S. Zhao, H. Ye, J. Yuan, P. Song, S. Hu, *J. Electroanal. Chem.* **2015**, *757*, 235–242.
[41] H. Xing, J. Xu, X. Zhu, X. Duan, L. Lu, W. Wang, *J. Electroanal. Chem.* **2016**, *760*, 52–58.
[42] M. Y. Pudza, Z. Z. Abidin, S. Abdul-rashid, F. Yasin, *Environ. Sci. Pollut. Res. Int.* **2020**, 13315–13324.
[43] L. Hermouche, Y. Aqil, K. Abbi, Y. El, F. Ouanji, S. Hajjaji, M. Mahi, E. Lotfi, N. Labjar, *Chem. Data Collect.* **2021**, *32*, 100642.

Received: March 11, 2022
Accepted: June 12, 2022
Published online on July 1, 2022

